ISSN 2095-9281 (网络)
ISSN 2095-9273 (印刷)
科学通报 (英文版)

Science Bulletin

Volume 70 · Number 14 · July 2025

ELSEVIER
SCIENCE CHINA PRESS
Chinese Academy of Sciences
National Natural Science Foundation of China

Science Bulletin xxx (xxxx) xxx

Contents lists available at ScienceDirect

Science Bulletin

journal homepage: www.elsevier.com/locate/scib

Short Communication

Juvenile macular degeneration in nonhuman primates generated by germline knockout of *ABCA4* gene

Ya Ma [a,1], Qiang Lin [a,b,1], Hai-Long He [a], Yi-Xin Liu [a], Min Li [a], Xiao-Hui Zhang [a], Zi-Bing Jin [a,*]

[a] Beijing Institute of Ophthalmology, Beijing Tongren Eye Center, Beijing Tongren Hospital, Capital Medical University, Beijing 100730, China
[b] Department of Physiology, School of Basic Medical Sciences, Wenzhou Medical University, Wenzhou 325035, China

ARTICLE INFO

Article history:
Received 31 March 2025
Received in revised form 21 April 2025
Accepted 27 April 2025
Available online xxxx

The macula, a cone photoreceptor-dense region critical for high-acuity vision, undergoes pathological degeneration in Stargardt disease type 1 (STGD1), an autosomal recessive juvenile disorder characterized by genetic heterogeneity and variable clinical manifestations. Pathogenesis is predominantly attributed to mutations in *ABCA4*, which disrupt retinal pigment epithelium (RPE) homeostasis through toxic lipofuscin accumulation, inducing apoptosis and subsequent photoreceptor loss [1–3].

The development of effective therapies is critically hindered by the financial burden of clinical trials and the scarcity of *ABCA4*-affected patients, underscoring the necessity for robust preclinical models. Animal models that authentically replicate human STGD1 pathophysiology remain indispensable for mechanistic exploration and therapeutic validation. While rodent and canine models exhibit limitations in phenocopying human macular degeneration, non-human primates (NHPs) offer unparalleled advantages due to their anatomical and physiological retinal similarities to humans, establishing them as the gold standard for translational ocular research [4,5]. Developing an NHP model of STGD1 would significantly advance both basic mechanistic studies and preclinical evaluation of gene- and cell-based therapies.

Current NHP models possess inherent limitations that constrain their utility in macular degeneration [6–9]. For instance, adeno-associated virus-mediated clustered regularly interspaced short palindromic repeats/CRISPR-associated protein 9 (AAV-mediated CRISPR/Cas9) somatic gene knockout [6,7], while achieving moderate editing efficiency, suffers from transient efficacy, often failing to sustain long-term phenotypic changes. Additionally, suboptimal delivery efficiency to target tissues further limits its applicability. Moreover, Somatic editing in adults cannot address gene functions critical during embryonic or early developmental stages, precluding the investigation of congenital disorders or neurodevelopmental diseases. Finally, somatic edits cannot stably transmit genetic modifications to offspring, necessitating repeated interventions for each animal ultimately resulting in compromise of the individual heterogeneity. In contrast, germline-edited NHP models introduce mutations at the one-cell stage, ensuring that genetic edits are present in all somatic and germline cells, thereby eliminating mosaicism and enabling stable phenotypic outcomes. By targeting genes from conception, such models capture the full spectrum of developmental effects, making them ideal for studying early-onset diseases or genes with critical roles in embryogenesis. Furthermore, the heritable nature of germline edits allows for colony expansion through breeding, establishing genetically uniform cohorts thus contribute to the preclinical research on human diseases.

In the present study approved by the animal experimental ethics board of the Ethics Committee (approval No. K001116023-02,01) at an Association for Assessment and Accreditation of Laboratory Animal Care (AAALAC) accredited facility-Kunming Biomed International (KBI, Yunnan Province, China), we used zygotic injection of CRISPR/Cas9 to target exon 2 and exon 6 of *ABCA4,* respectively at one-cell stage of cynomolgus monkeys (*M. fascicularis*) (Fig. 1a and Fig. S1a online). The CRISPR/Cas9 system (Tables S1 and S2 online) was tested at the embryo level and achieved a high efficiency (93.75%) (Fig. S1b, c and Table S3 online). We microinjected 28 zygotes after *in vitro* fertilization and transferred into 8 surrogate females, resulting in four pregnancies of two twins and two monocyesis, respectively (Fig. 1a). Unfortunately, three surrogate female monkeys were aborted at early gestation. Finally, we performed C-section at 160-d gestation for a surrogate female with twins, leading to a live male monkey and a female monkey (Fig. 1a). Sanger sequencing revealed the female monkey was homozygous knockout at exon2 (Fig. S1d online) (termed $ABCA4^{-/-}$ M#2 below) and the male monkey was both heterozygous knockout at exon 2 and exon 6 (Fig. S1e, f online) (termed $ABCA4^{exon2/-:exon6/-}$ M#1 below). The

* Corresponding author.
E-mail address: jinzb502@ccmu.edu.cn (Z.-B. Jin).
[1] These authors contributed equally to this work.

https://doi.org/10.1016/j.scib.2025.04.077
2095-9273/

Please cite this article as: Y. Ma, Q. Lin, H.-L. He et al., Juvenile macular degeneration in nonhuman primates generated by germline knockout of *ABCA4* gene, Science Bulletin, https://doi.org/10.1016/j.scib.2025.04.077

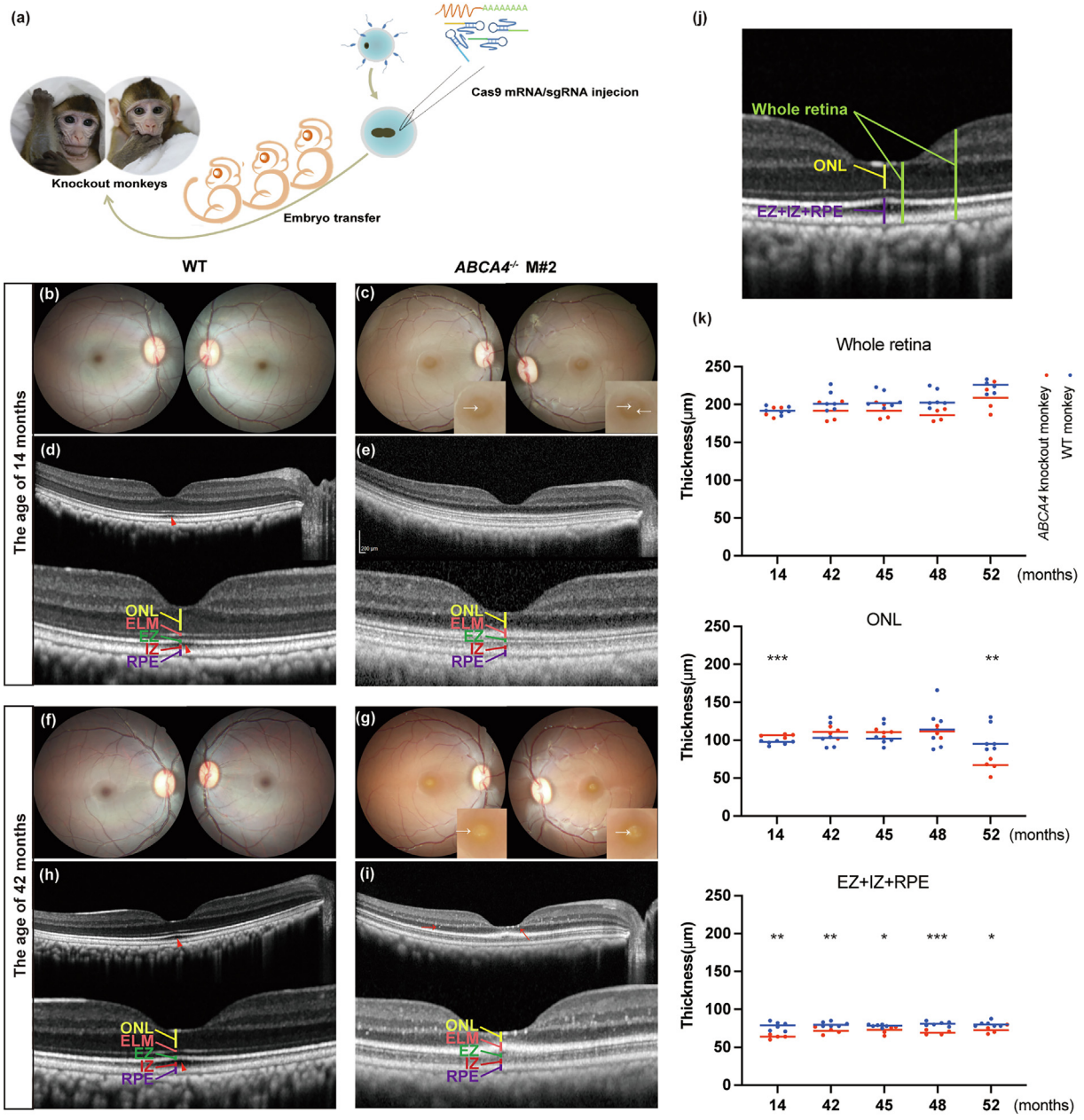

Fig. 1. Generation of *ABCA4* knockout monkeys and the continuous changing of retina structure. (a) Schematic illustration of generating the knockout monkeys. (b) Representative fundus photos of WT monkey at the age of 14 months. (c) Representative fundus photos of *ABCA4*$^{-/-}$ monkey #2 at the age of 14 months. Within the oval depigmented area at the fovea, a vague, yellow fleck can be seen bilaterally (indicated by arrow). (d) OCT image and zoomed-in central macular OCT image of WT monkeys. Layer segmentation was performed manually based on OCT and was indicated in different colors. The colored segments denote distinct retinal layers, with labels annotated adjacent to each corresponding segment: ONL: outer nuclear layer; ELM: external limiting membrane; EZ: ellipsoid zone; IZ: interdigitate zone; RPE: retinal pigment epithelium. The height of each segment corresponds to the thickness of the respective layer at the fovea. The outer segment lengthening was indicated by red triangle. (e) OCT image and zoomed-in central macular OCT image of *ABCA4* knockout monkey at the age of 14 months. Layer segmentations were indicated in different colors. The thickened ELM is maximally broadened at the foveola and attenuated around. The EZ was diminished. The IZ and RPE were preserved but with reduced clarity. The outer segment lengthening was absent. (f) Representative Fundus photos of WT monkey at the age of 42 months. (g) Representative Fundus photos of *ABCA4*$^{-/-}$ monkey #2 at the age of 42 months. Whitish dots or patches were seen inside the sharply demarcated yellow foveal lesion (indicated by arrow). (h) OCT image and zoomed-in central macular OCT image of WT monkeys at the age of 42 months. Layer segmentations were indicated in different colors. The outer segment lengthening was indicated by red triangle. (i) OCT image and zoomed-in central macular OCT image of *ABCA4* knockout monkey at the age of 42 months. Layer segmentations were indicated in different colors. The outer segment lengthening was absent. The thickened ELM became more discernible and broadened at foveola. Disruption of ellipsoid zone at foveola as well as faint IZ and RPE became more obvious. Multiple hyperreflective retinal spots were also noted in ONL (indicated by red arrow). (j) Schematic of retinal layers thickness. Retinal layers were measured based on OCT including ONL, EZ, IZ, RPE, and the whole retina thickness. (k) Comparison of retinal thickness at different age. The comparison between KO (n = 4, 2 individuals, 4 eyes) and WT (n = 6, 3 individuals, 6 eyes) at each time point was performed with t-test and the P-value was hinted in the figure with $^{*}P < 0.05$; $^{**}P < 0.01$; $^{***}P < 0.001$.

whole genome sequencing (WGS) confirmed the CRISPR/Cas9-editing status (Fig. S2 online) and identified that there was a heterozygous 5-bp insertion at exon 6 in *ABCA4*$^{-/-}$ M#2 (Fig. S2a online). These indels were not multiples of three nucleotides in length, thereby inducing frameshift mutations in the open reading frame of *ABCA4* that disrupt gene function. The exon2 was thirteen thousand base pairs away from exon 6, we failed to verify whether the knockouts were generated in the same chromosome or not in

ABCA4$^{exon2/-:exon6/-}$ M#1. Inspiringly, both monkeys showed the typical phenotype of early-stage STGD1. We speculated that the heterozygous knockouts in *ABCA4*$^{exon2/-:exon6/-}$ M#1 may be located in two homologous chromosomes thus we generated an *ABCA4* knockout male monkey. Three developmental-stage-matched wild-type (WT) monkeys were recruited for comparison (Table S4). For the off-target effect, the WGS displayed a small number of *de novo* mutations, which could be explained by spontaneous mutations or random errors in sequencing reads (Figs. S3 and S4 and Table S5 online), and no other unexpected off-target mutations were detected consistent with the previous report [10].

We performed clinical ophthalmic examinations to record the continuous progress of retinal changes, including fundus photography, fundus autofluorescence imaging (FAF), and optical coherence tomography (OCT) in *ABCA4* knockout monkeys. An oval demarcated depigmented area at the fovea was found bilaterally in knockout monkeys and aggravated to be a lesion with whitish dots or patches inside through development in tune with vague high signal flecks on FAF (Fig. 1b, c, f, g and Fig. S5 online). The thickened external limiting membrane (ELM) which has been reported as one of the early structural changes in *ABCA4*-defected patients [11] was observed at the age of 14 months with markedly increased reflectivity on OCT and became more discernible as developing progresses goes on (Fig. 1d, e, h, i). The ellipsoid zone (EZ) was diminished and finally disrupted at the foveola (Fig. 1d, e, h, i). The interdigitation zone (IZ) and RPE were preserved but faint on OCT (Fig. 1d, e, h, i). In addition, the absence of outer segment lengthening was also noted since the age of 14 months (Fig. 1d, e, h, i). For a better understanding possible progress pattern of *ABCA4*-defected associated macular degeneration in clinical, a diagram was depicted with two representative OCT images of *ABCA4*-associated retinopathy patients at preclinical and clinical stages, respectively (Fig. S6a online). The structure of each layer was preserved at the beginning. Gradually, the retinal abnormality aggravated and the disruption of outer retina emerged. When the disease progressed into the clinical stage, obvious disruption of outer retinal layers arose. The *ABCA4*-associated retinopathy patient at the preclinical stage exhibited obvious ELM thickening and EZ diminishing (Fig. S6a online, upper right). As the disease progresses, the retina thinning gradually, the outer retinal layer irregulation and subretinal debris arise (Fig. S6a online, bottom right). The dynamic development of retina of *ABCA4* knockout monkeys was consistent with the early pathologic course of *ABCA4*-defected STGD1 patients indicating that our *ABCA4* knockout monkeys are still at the primary stage of disease (Fig. S6b online).

To quantify the changes in retinal layer thickness, the thickness of the whole retina, ONL and EZ+IZ+RPE were measured based on OCT (Fig. 1j and Fig. S7a online). There was no significant change found in the thickness of the whole retina of *ABCA4* knockout monkeys during development (Fig. 1k upper and Fig. S7b online). As the progress goes on, the thickness of ONL dramatically decreased at the age of 52 months, suggesting the apoptosis of photoreceptors (Fig. 1k middle and Fig. S7b online). The thickness of ONL at the fovea in knockout monkeys was significantly thicker at the age of 14 months and the difference disappeared as development progressed until the age of 52 months (Fig. 1k middle and Fig. S7b online). It was rarely reported that *ABCA4*-defected patients possessed a thicker ONL at the early stage in clinical. As the disease progressed, the photoreceptors began to undergo apoptosis and the ONL became thinner (Fig. 1k middle). The thickness of the layer of EZ+IZ + RPE showed a tendency to increase with age, except for it at the fovea (Fig. S7b online). Significant decrease of EZ+IZ+RPE thickness at the fovea was found in *ABCA4* knockout monkeys at each time point (Fig. 1k bottom). It was consistent with the interruption of EZ and IZ since the age of 14 months.

To delineate the functional consequence of germline knockout of *ABCA4* in NHP, the full-field electroretinography (ffERG) was performed at the ages of 42, 45, and 52 months. In ffERG, dark-adapted response at low intensity (0.01 and 3.0) presents the function of rod photoreceptors and the higher intensity (10.0) presents the mixed rod-cone photoreceptor reaction. Light-adapted response presents the function of cone photoreceptors. At the age of 42 months, the dark-adapted amplitude of a wave was lower in *ABCA4* knockout monkeys indicating rod dysfunctions while the function of cones remained intact (Fig. 2a). The dysfunction of cone and rod photoreceptors progressively aggravated since rod response, cone response and mixed response were decreased at the age of 45 months and continuously deteriorated till to the age of 52 months (Fig. 2b, c) consistent with the structure changes detected in OCT in knockout monkeys. These results hinted that the dysfunction of rod photoreceptors prior to cone photoreceptors at the early stage and progressive deterioration of photoreceptors with age. These evidences further verified our *ABCA4* knockout NHP models were still at the primary stage of the disease and sustained suffering retinal degeneration with age.

There were currently no proven cures for STGD1 due to its genetic and clinical heterogeneity. Though several treatment avenues including pharmacological agents [12], gene therapy [13] and stem cell therapy [14] are being investigated in clinical trials, their pre-clinical studies were mostly based on macular-free animals leading to the omission of important details in research and making it hard to accurately assess the efficacy and safety.

Our germline knockout NHP models ensure ubiquitous and non-mosaic knockout across all retinal cells, including photoreceptors and RPE—key cell types affected in Stargardt disease. By recapitulating the developmental onset and pan-retinal pathology of STGD1, this model overcomes critical limitations of existing rodent or postnatal NHP models, which often fail to fully mimic human disease progression due to anatomical, physiological, or genetic disparities, representing a transformative advance in preclinical research for inherited macular degeneration disorders. Our NHP models bridges a critical gap between proof-of-concept studies in cell lines or rodents and human trials by providing a physiologically and genetically faithful platform for evaluating gene therapy approaches, including AAV-based gene therapy and induced pluripotent stem cell-based therapies, thus enabling systematic testing of delivery strategies, optimization of therapeutic dosage, and comprehensive assessment of long-term safety. It is critical to acknowledge that we generated only two *ABCA4* knockout NHP models which restrict statistical power and generalizability, as observed phenotypic variations may reflect individual differences rather than universal biological mechanisms. Fortunately, both animals exhibited phenotypic features of STGD1, with consistent trends in phenotypic progression observed across all subjects. The limitation should be addressed in future studies through expanded cohorts. Furthermore, as sequence variants in *ABCA4* are a known cause of STGD1, the model's application in preclinical research offers valuable insights for emerging therapeutic approaches, such as prime editing (PE) [15] and adenine base editing (ABE) [16], to correct single-nucleotide mutations.

Collectively, to the best of our knowledge, we for the first time well established the macular degeneration NHP models with STGD1 by the germline knockout of *ABCA4*. These models phenocopied key features of human STGD1, such as thickened ELM, attenuated or disrupted EZ, and photoreceptor dysfunction. Our models were born to be pathogenic and are still at the early stage of retina degeneration, so that we could schedule ophthalmic examination windows to continuously record disease progression

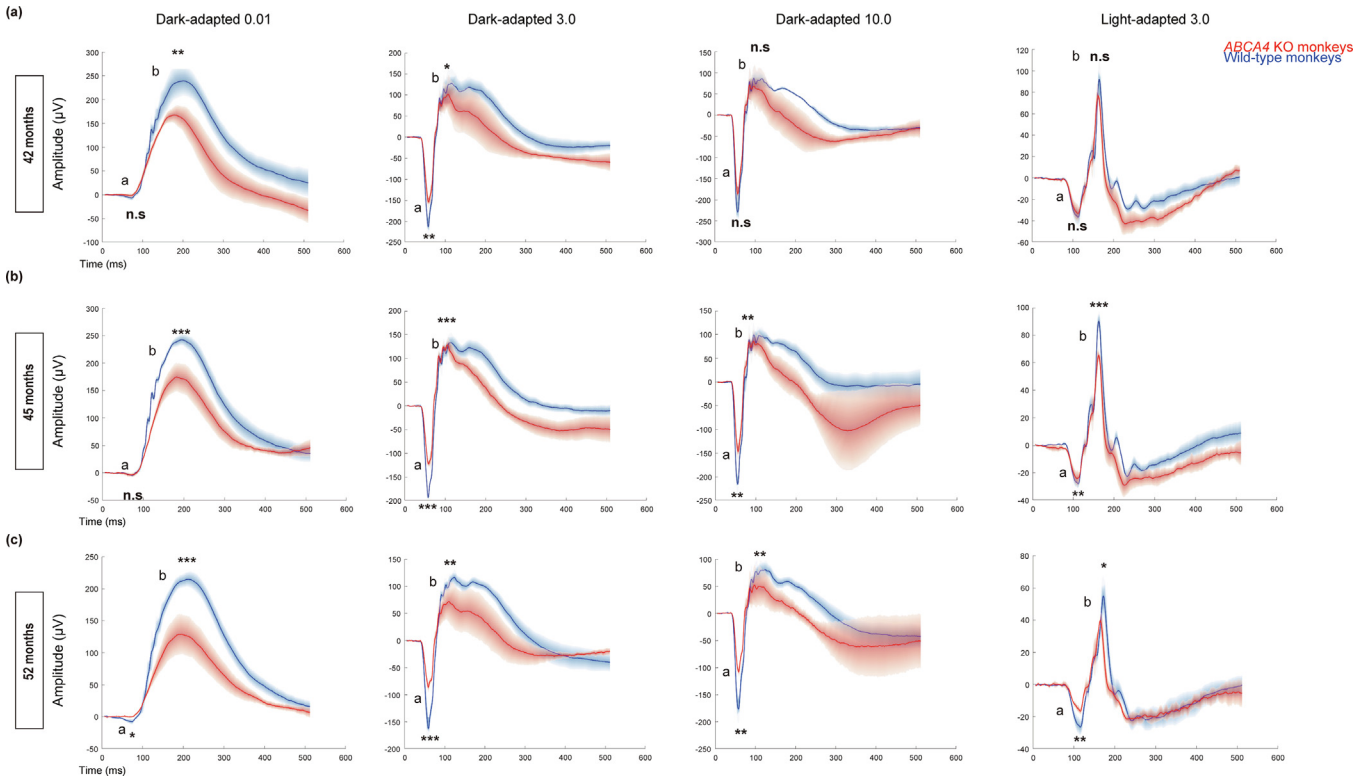

Fig. 2. Full-field electroretinography of *ABCA4* KO and WT monkeys. The red tracings indicate *ABCA4* knockout monkeys, while the blue ones indicate wild-type monkeys. (a) The dark-adapted 0.01, 3.0, 10.0, and light-adapted 3.0 responses of both groups at the age of 42 months. (b) The dark-adapted 0.01, 3.0, 10.0, and light-adapted 3.0 responses of both groups at the age of 45 months. (c) The dark-adapted 0.01, 3.0, 10.0, and light-adapted 3.0 responses of both groups at the age of 52 months. The a wave and b wave were indicated in the figure. The comparison between KO (n = 4, 2 individuals, 4 eyes) and WT (n = 6, 3 individuals, 6 eyes) of a wave and b wave was performed with t-test and the P-value was hinted in the figure with $^{*}P < 0.05$; $^{**}P < 0.01$; $^{***}P < 0.001$.

and avoid missing any details during pathogenesis. Fortunately, our NHP models are capable of mating and reproduction, albeit at a slow rate, the bottleneck of insufficient pre-clinical NHP models of STGD1 could be addressed.

This germline knockout STGD1 model is not merely incremental but paradigm-shifting, offering a robust, human-relevant system to validate next-generation gene therapies. It addresses the Achilles' heel of traditional models—lack of developmental and genetic fidelity—and positions NHPs as indispensable for advancing curative treatments for STGD1 and other monogenic disorders.

Conflict of interest

The authors declare that they have no conflict of interest.

Acknowledgments

This work was partly supported by the National Natural Science Foundation of China (82125007 and 92368206), the Beijing Natural Science Foundation (Z200014), Beijing Municipal Public Welfare Development and Reform Pilot Project for Medical Research Institutes (PWD&RPP-MRI and JYY2023-6) and the Dengfeng Program of Beijing Hospitals Authority (DFL20220202), and the Youth Beijing Scholar program. We thank Drs. Xiao-Yan Peng and Jing-Hua Liu for the helpful discussion, Dan-Dan Shi for the assistance on the analysis of OCT data.

Author contributions

Zi-Bing Jin designed and supervised the overall study, provided financial support. Ya Ma, Qiang Lin, and Hai-Long He performed experiments. Qiang Lin, Ya Ma, and Min Li performed data analysis. Xiao-Hui Zhang acquired information and OCT images of the *ABCA4* patient. Ya Ma, Qiang Lin, and Yi-Xin Liu drafted the manuscript. Zi-Bing Jin revised the manuscript.

Appendix A. Supplementary material

Supplementary data to this article can be found online at https://doi.org/10.1016/j.scib.2025.04.077.

References

[1] Strauss R W, Ho A, Munoz B, et al. The natural history of the progression of atrophy secondary to Stargardt disease (ProgStar) studies: design and baseline characteristics: ProgStar report no. 1. Ophthalmology 2016; 123: 817-828.
[2] Tsang SH, Sharma T. Stargardt disease. Ad Exp Med Biol 2018;1085:139–51.
[3] Molday RS, Garces FA, Scortecci JF, et al. Structure and function of *ABCA4* and its role in the visual cycle and Stargardt macular degeneration. Prog Retin Eye Res 2022;89:101036.
[4] Bringmann A, Syrbe S, Gorner K, et al. The primate fovea: structure, function and development. Prog Retin Eye Res 2018;66:49–84.
[5] Wu KC, Lv JN, Yang H, et al. Nonhuman primate model of oculocutaneous albinism with *TRY* and *OCA2* mutations. Research 2020;2020:1658678.
[6] Li S, Hu Y, Li Y, et al. Generation of nonhuman primate retinitis pigmentosa model by in situ knockout of RHO in rhesus macaque retina. Sci Bull 2021;66:374–85.
[7] Lin Q, Lv JN, Wu KC, et al. Generation of nonhuman primate model of cone dysfunction through *in situ* AAV-mediated *CNGB3* ablation. Mol Ther Methods Clin Dev 2020;18:869–79.
[8] Ikeda Y, Nishiguchi KM, Miya F, et al. Discovery of a cynomolgus monkey family with retinitis pigmentosa. Invest Ophthalmol Vis Sci 2018;59:826–30.
[9] Peterson SM, McGill TJ, Puthussery T, et al. Bardet-Biedl syndrome in rhesus macaques: a nonhuman primate model of retinitis pigmentosa. Exp Eye Res 2019;189:107825.
[10] Luo X, He Y, Zhang C, et al. Trio deep-sequencing does not reveal unexpected off-target and on-target mutations in Cas9-edited rhesus monkeys. Nat Commun 2019;10:5525.

[11] Khan KN, Kasilian M, Mahroo OAR, et al. Early patterns of macular degeneration in ABCA4-associated retinopathy. Ophthalmology 2018;125:735–46.
[12] Dugel PU, Novack RL, Csaky KG, et al. Phase II, randomized, placebo-controlled, 90-day study of emixustat hydrochloride in geographic atrophy associated with dry age-related macular degeneration. Retina 2015;35:1173–83.
[13] Parker MA, Erker LR, Audo I, et al. Three-year safety results of SAR422459 (EIAV-ABCA4) gene therapy in patients with ABCA4-associated Stargardt disease: an open-label dose-escalation phase I/IIa clinical trial, cohorts 1-5. Am J Ophthalmol 2022;240:285–301.
[14] Li SY, Liu Y, Wang L, et al. A phase I clinical trial of human embryonic stem cell-derived retinal pigment epithelial cells for early-stage stargardt macular degeneration: 5-years' follow-up. Cell Prolif 2021;54:e13100.
[15] Anzalone AV, Randolph PB, Davis JR, et al. Search-and-replace genome editing without double-strand breaks or donor DNA. Nature 2019;576:149–57.
[16] Gaudelli NM, Komor AC, Rees HA, et al. Programmable base editing of A•T to G•C in genomic DNA without DNA cleavage. Nature 2017;551:464–71.

Juvenile macular degeneration in nonhuman primates generated by germline knockout of *ABCA4* gene

Materials and methods

SgRNA design. sgRNAs target exon2 and exon6 were designed according to the CRISPR design web tool (https://zlab.bio/guide-design-resources). For each exon, the two sgRNAs targeted the sense and antisense strands respectively. For exon2, the sgRNAs target region cover the whole exon. For exon6, the distance between two sgRNAs is 76bp, it was optimal distance for two sgRNAs targeting the same gene.

Cas9 mRNA and sgRNA In vitro transcription. The selected sgRNAs were cloned into *PUC57-sgRNA* vector (Addgene No. 51132) respectively. The sgRNAs were transcribed according to the manufacturer's instructions of the MEGAshortscript Kit (Ambion, AM1354) after the vectors were linearized by digestion with DraI (NEB, R0129S). Then SgRNAs were purified according to the manufacturer's instructions of the MEGAclear Kit (Ambion, AM1908). Cas9 mRNA was transcribed according to the manufacturer's instructions of the T7 Ultra Kit (Ambion, AM1345) after the pST1374-Cas9-NLS-flag-linker vector (Addgene No. 44758) was linearized with AgeI (NEB, R0552S) digestion. The Cas9 mRNA was purified according to the manufacturer's description of the RNeasy Mini Kit (Qiagen, 74104).

Zygote injection, embryo test and transfer. Briefly, superovulation was administrated on healthy female monkeys in regular menstrual cycle by intramuscular injection with rhFSH (Recombinant Human Follitropin Alfa, Merck Serono) for continuous 8 days. Then rhCG (Recombinant Human Chorionic Gonadotropin Alfa,

Merck Serono) was injected on the next day. 36h later, the oocytes were harvested by laparoscopic follicular aspiration. The MII oocytes were selected for in vitro fertilization and the status was confirmed by the presence of two pronuclei. Fertilized eggs were then injected with a mixture of Cas9 mRNA (100 ng/μl), sgRNA1 (50 ng/μl), sgRNA2 (50 ng/μl), sgRNA7 (50 ng/μl) and sgRNA12 (50 ng/μl) into cytoplasm using a Nikon microinjection system. Then the zygotes were cultured in the chemically defined, protein-free hamster embryo culture medium-9 (HECM-9) containing 10% fetal calf serum (HycloneLaboratories, SH30088.02) at 37 ℃, 5% CO_2. For embryo test, embryos were harvested immediately when they stop ontogeny or culture in a week. Every single embryo was transfer into a single tube. For embryos transfer, the normally developed embryos from 2-cell to 8-cell with high quality were transferred into the oviduct of matched recipients. A total of eight monkeys were selected as surrogate. Typically, two embryos were transferred into the same recipient female. The pregnancy status could be diagnosed with ultrasonography 30 days after transfer.

Embryo test and TA-clone seq. Add 50μl alkaline lysis solution (25 mM NaOH, 0.2 mM EDTA; pH ~ 12) into the embryo tube and heated the tube for 10min at 98 ℃. Replace the tube onto ice immediately after the heating. Add 50μl neutralizing solution (40 mM Tris.HCl; pH ~ 5) into the tube and mixed thoroughly. Then the supernate could be used as the template. We amplified the target region from two round of PCR. The primer used was list in Table S6. Taken 1μl of the neutralizing supernate as the template amplified with nest primer pair 1. The steps were as fellow:

95 ℃ for 5 min; 95 ℃ for 30s, 62 ℃ for 30s, 72 ℃ for 30s, go for 10 cycles; 72 ℃ for 2 min. The pre-amplified product could be used as the template of second round PCR. The second PCR was performed with nest primer pair 2. The steps were as fellow: 95 ℃ for 5 min; 95 ℃ for 30s, 64 ℃ for 30s, 72 ℃ for 30s, go for 35 cycles; 72 ℃ for 3 min. The products were purified and subcloned into pMD19 vector (Takara, 3271). The colonies were picked up randomly and sequenced by M13-F primer. At least 10 colonies were picked for every embryo.

DNA extraction and genotype of *ABCA4* knockout monkeys. A little ear tissue was sampled after the monkeys were born. Genomic DNA was extracted using the DNeasy Blood & Tissue Kit (Qiagen, 69506) according to manufacturer's instructions. The nest primer pair 2 could be used to amplified the exon 2 and exon 6 respectively. PCR products underwent Sanger sequencing after they were purified. If there was double peak appeared at the same position, then TA clone was performed to verify the genotype of the embryo. At least ten colonies were sequenced by M13-F primer.

Whole-genome sequencing (WGS) and potential off-target effect. DNA libraries were constructed using standard protocols for the Illumina platform. Briefly, 100ng DNA underwent fragmented, size selection(300-400bp), end-repaired, A-tailed, and adapter ligated. Libraries were then sequenced by Illumina X10 as paired-end 150 base reads. We generated on average 0.7 billion raw reads per monkey and the mean Q30 of read-pairs are higher than 94% resulting in a median depth>36×. For the potential off-target effect detection, we performed BLAST for four sgRNAs against the genome to screen for potential off-target sites. Except for sgRNA3, which

exhibited a single unique hit, the other three sgRNAs showed theoretical off-target sites. From these results, we selected sites overlapping with coding genes (Table S5) and further examined them using whole-genome data, expanding the search range to 20 bp upstream and downstream of each site (total 60 bp). No significant indels were detected in these regions, except for sporadic point mutations attributable to spontaneous mutations or random errors in sequencing reads (Fig. S3-S4). Therefore, our NHP models did not exhibit detectable off-target effects, consistent with previous finding [2].

Animals. All animals were housed at an Association for Assessment and Accreditation of Laboratory Animal Care (AAALAC) accredited facility-Kunming Biomed International (KBI, Yunnan Province, China). The protocol was approved by the animal experimental ethics board of the Ethics Committee (Approval NO. K001116023-02,01). For Surrogate Monkeys, after C-section, the surrogates were transferred to a well-controlled recovery chamber until full consciousness and stable vital signs were confirmed. Surgical incisions were treated with topical iodine-based antiseptics and systemic prophylactic antibiotics were performed twice daily for 7 days. Buprenorphine (0.01 mg/kg, subcutaneous, every 8–12 hours) was provided for 48 hours post-surgery to mitigate discomfort. Non-steroidal anti-inflammatory drugs (NSAIDs; meloxicam, 0.2 mg/kg, oral, daily) were administered for 7 days. The offspring were transfer to well-controlled nursery box and manual feeding every two hours with milk until 12 months. Umbilical cords were disinfected with chlorhexidine gluconate (2%) until healed. At the age of 12 month, the monkeys were transfer to the

animal cage and undergo normal diet. The monkeys were weighed monthly and subjected to a neonatal viability assessment. All the ophthalmic examinations were performed followed the guidelines of the ARVO Statement for the Use of Animals in Ophthalmic and Vision Research.

Examinations procedures. Three age-matched healthy cynomolgus monkeys were set as controls. The five cynomolgus monkeys were fasted and water-deprived for eight hours before examinations. Anesthesia was achieved by intramuscular injection of 50 mg/mL ketamine and 0.5 mg/mL atropine. All examinations were done by skilled ophthalmologists and finished in 120 minutes under anesthesia. Monkeys were monitored by an experienced veterinarian at all times. 1% tropicamide eye drops were used to dilate pupils. 0.4% Oxybuprocaine hydrochloride eye drops were used for local anesthesia during electroretinography. Eye speculum was used, and sodium hyaluronate eye drops were applied to maintain the corneal hydration.

Full-field electroretinography (ERG) was arranged at 42 months of age and repeated every 3 months later (45 months and 48 months). Full-field ERG was performed according to International Society for Clinical Electrophysiology of Vision (ISCEV) standards [1]. Monkeys were pre-adapted to dark for 20 minutes before tests began. ERG tests were recorded with contact lens after sufficient pupil dilatation and local anesthesia. Reference electrodes were placed on the brow arch with a hypodermic needle electrode, and ground electrode was positioned on the back. All electrode impedances were maintained below 5 MΩ. For each test, averaging after 5 to 10 stimulations were carried out to reduce variability and background noise.

Fundus examinations of the twins were arranged at 14 months, 42 months, 45 months and 48 months of their age. Fundus photographs were acquired by digital retinal camera (Canon CX-1, Tokyo, Japan) with 45° field centered on macula. Fundus fluorescence angiography (FFA), fundus autofluorescence (FAF) and optical coherence tomography (OCT) images were acquired by Heidelberg Retina Angiograph 2 or Heidelberg Spectralis (Heidelberg Engineering, Heidelberg, Germany). 20mg/kg 10% sodium fluorescein was injected into a vein in the leg.

Retinal layer thickness was assessed by built-in software on a horizontal line scan through the foveal center. Each layer thickness was measured at the fovea, 0.5mm, 1mm, 1.5mm and 2mm nasal and temporal to fovea. The layers measured included outer nuclear layer (ONL), ellipsoid zone (EZ), interdigitate zone (IZ), retinal pigment epithelium (RPE), and total retinal thickness.

Image J software (version 1.48; National Institutes of Health, USA) was used to measure macular lesion. Fundus photos were processed with enhanced contrast first, then macular lesion was delineated and measured by two independent, blinded, well-trained observers (Y.M. and Q.L.). Average data were used for the final analysis.

Statistical methods. Outcomes of OCT measurements were compared between *ABCA4* KO monkeys with controls. Statistical analysis was performed using the SPSS-for-Windows software (version 23.0; IBM-SPSS, Chicago, IL, USA). Independent sample t-test was used to compare variables between groups. One-way ANOVA with Bonferroni correction was used to assess the differences among groups. *P*-values represented results for 2-sided tests, with values less than 0.05 considered

statistically significant.

Reference

[1] Robson A G, Frishman L J, Grigg J, et al. Iscev standard for full-field clinical electroretinography (2022 update). Doc Ophthalmol 2022; 144: 165-177

[2] Luo X, He Y, Zhang C, et al. Trio deep-sequencing does not reveal unexpected off-target and on-target mutations in cas9-edited rhesus monkeys. Nat Commun 2019; 10: 5525.

Supplementary figures

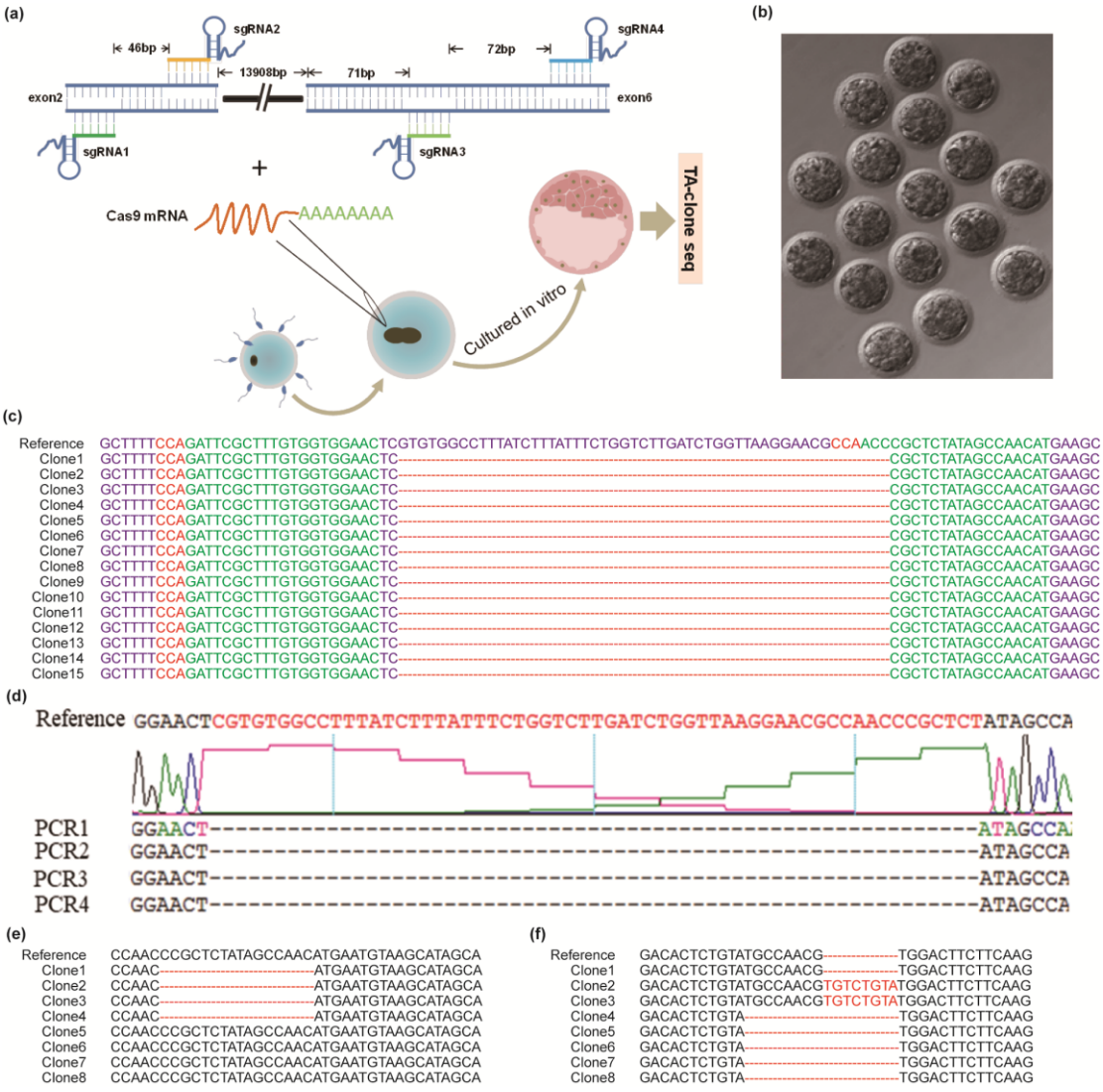

Fig. S1 Efficiency test of CRISPR/Cas9 system in embryos and the genotype of *ABCA4* knockout monkeys. (a) The design of CRISPR/Cas9 system targeting *ABCA4*. **(b)** Invitro cultured embryos after injection **(c)** Representative clone

sequencing of injected embryo. The PAM sequence was showed in red. The target sequence was showed in green. **(d)** PCR Sanger sequencing of *ABCA4* exon2 of the female monkey. **(e-f)** TA-clone sequencing result of *ABCA4* exon2 and exon6 of the male monkey.

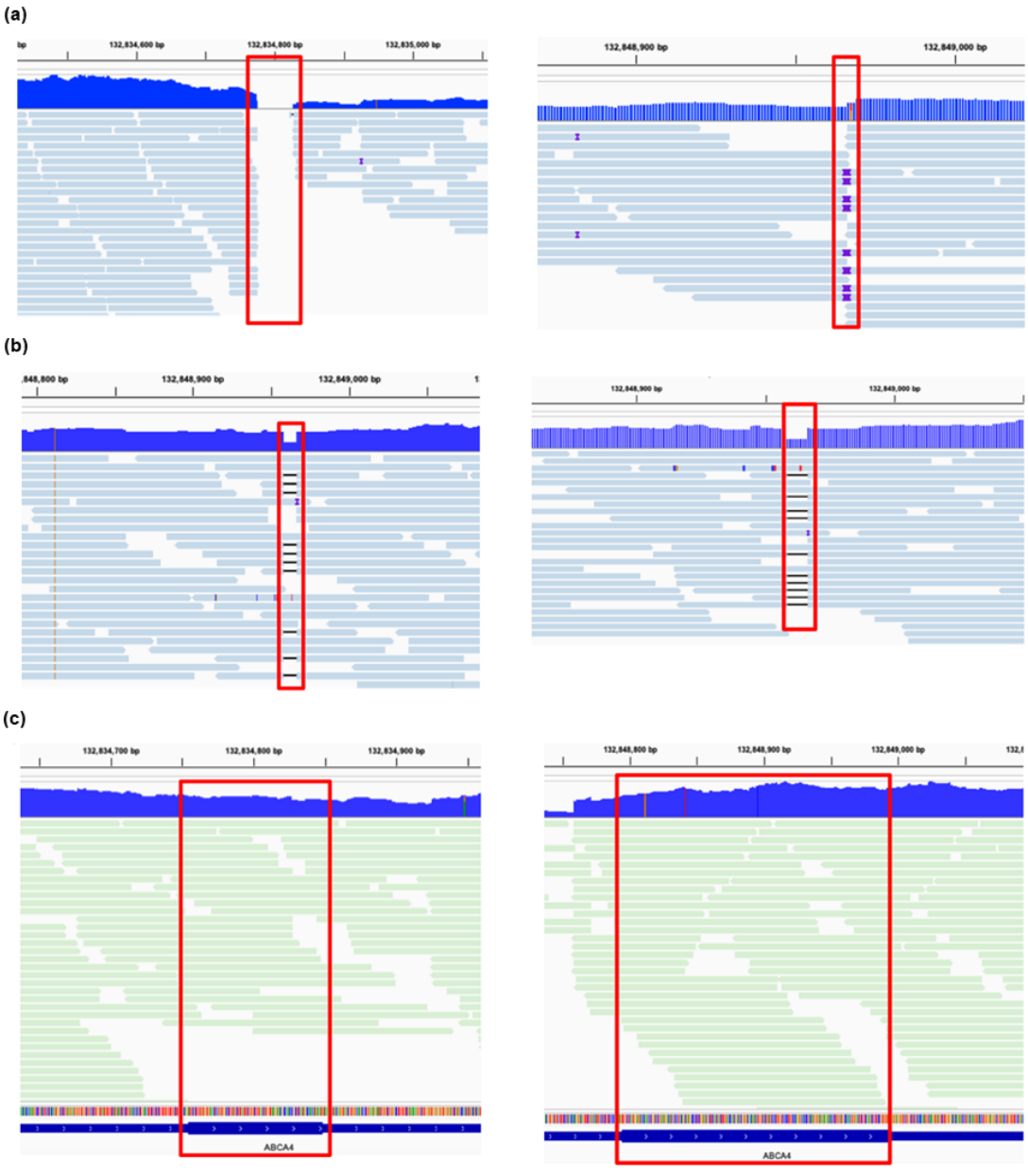

Fig. S2 The integrative genomics view of *ABCA4* exon2 and exon6 of the monkeys. (a) Integrative genomics view of *ABCA4* exon2 and exon6 of the female monkey. The target region was indicated in red box. **(b)** Integrative genomics view of

ABCA4 exon 2 and exon6 of the male monkey. The target region was indicated in red box. **(c)** Integrative genomics view of *ABCA4* exon 2 and exon6 of WT monkey. The red box highlights the entire exon2 and exon6.

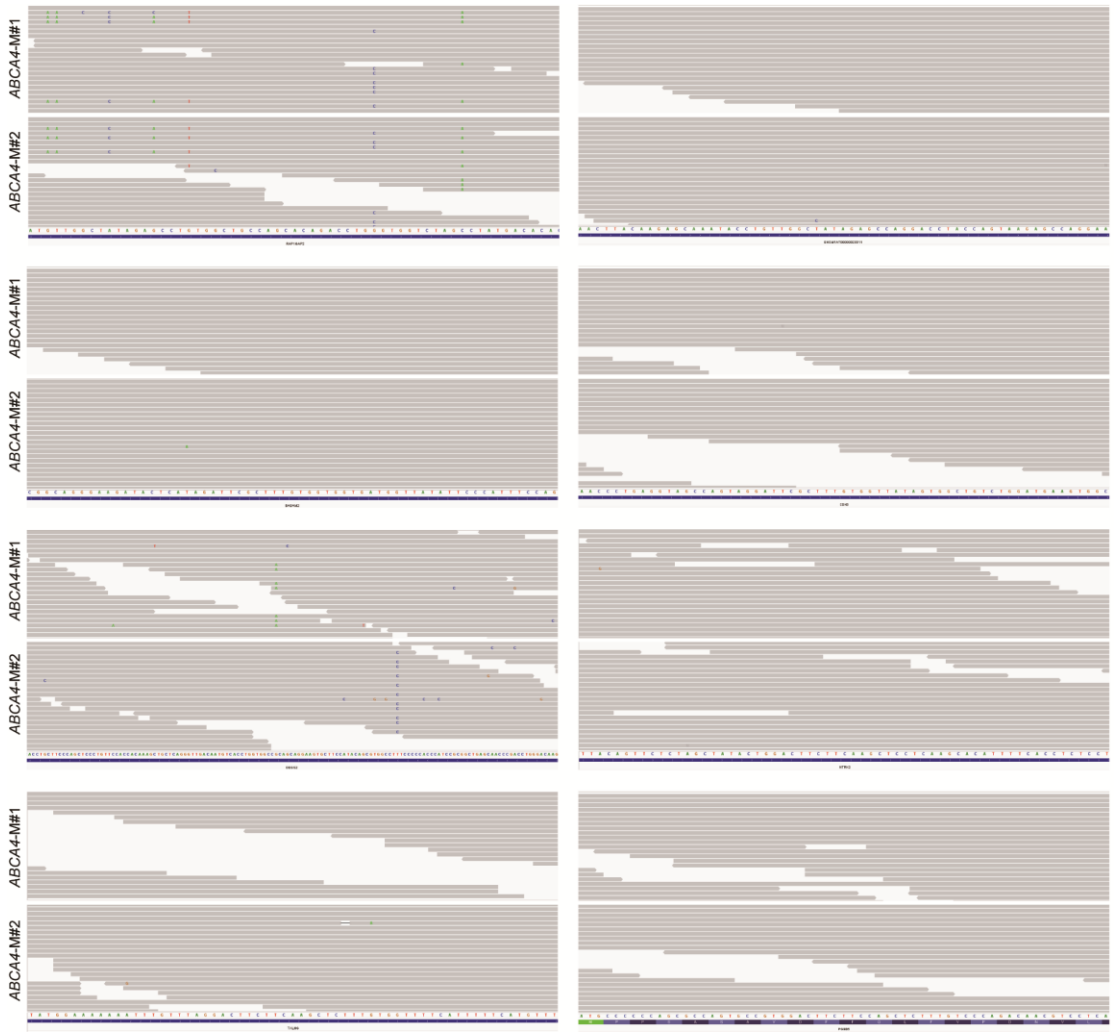

Fig. S3 The integrative genomics view of potential off-target site (part 1). Each small panel corresponds to one off-target site in each of the two knockout monkeys, with sequence extended 20 bp upstream and downstream respectively. Gray lines represent individual sequencing reads, and mismatches are highlighted in reads with colored A/T/C/G. The nucleotide sequence and overlapping genes were labeled at the bottom of each panel. The result showed there were no significant indels in these regions, except for sporadic point mutations.

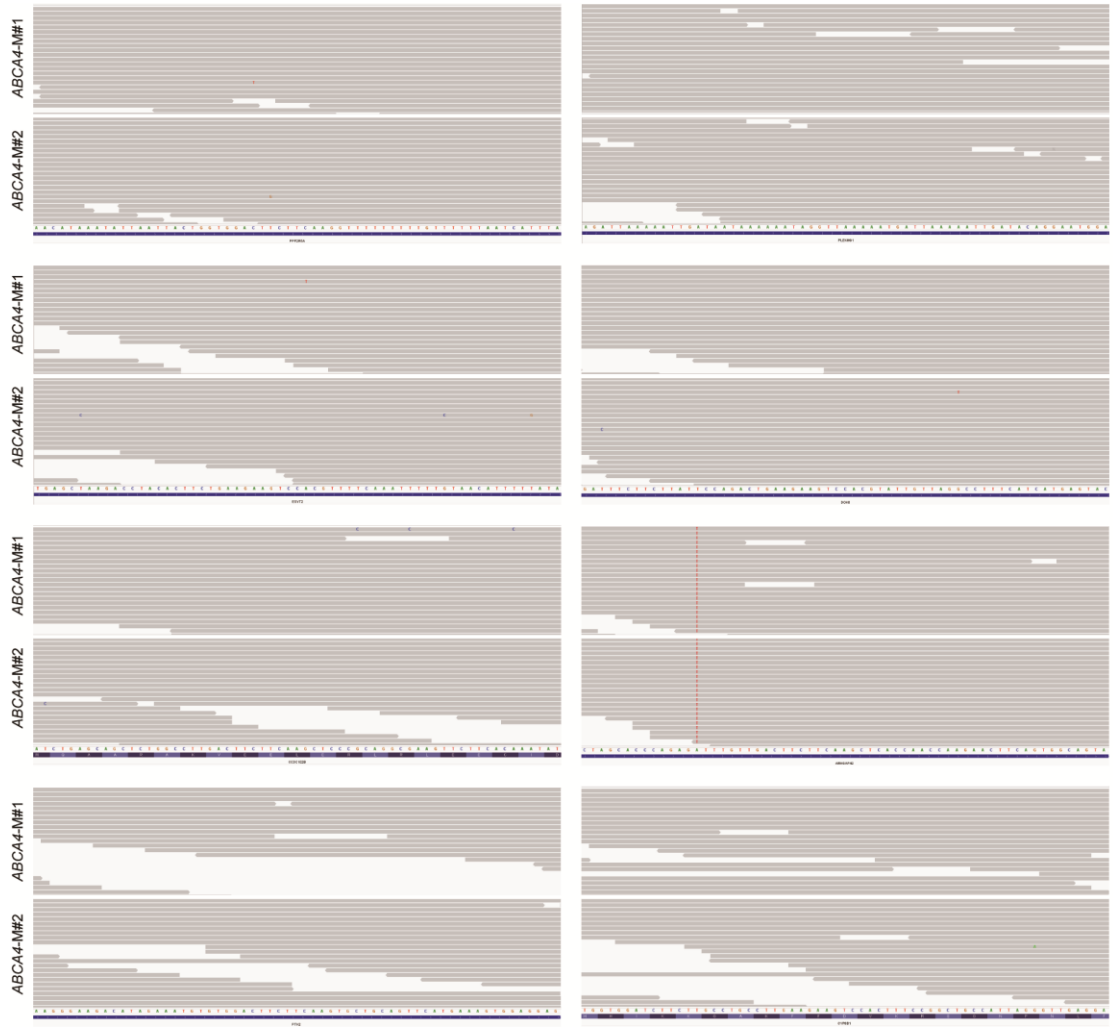

Fig. S4 The integrative genomics view of potential off-target site (part 2). Each small panel corresponds to one off-target site in each of the two knockout monkeys, with sequence extended 20 bp upstream and downstream respectively. Gray lines represent individual sequencing reads, and mismatches are highlighted in reads with colored A/T/C/G. The nucleotide sequence and overlapping genes were labeled at the bottom of each panel. The result showed there were no significant indels in these regions, except for sporadic point mutations.

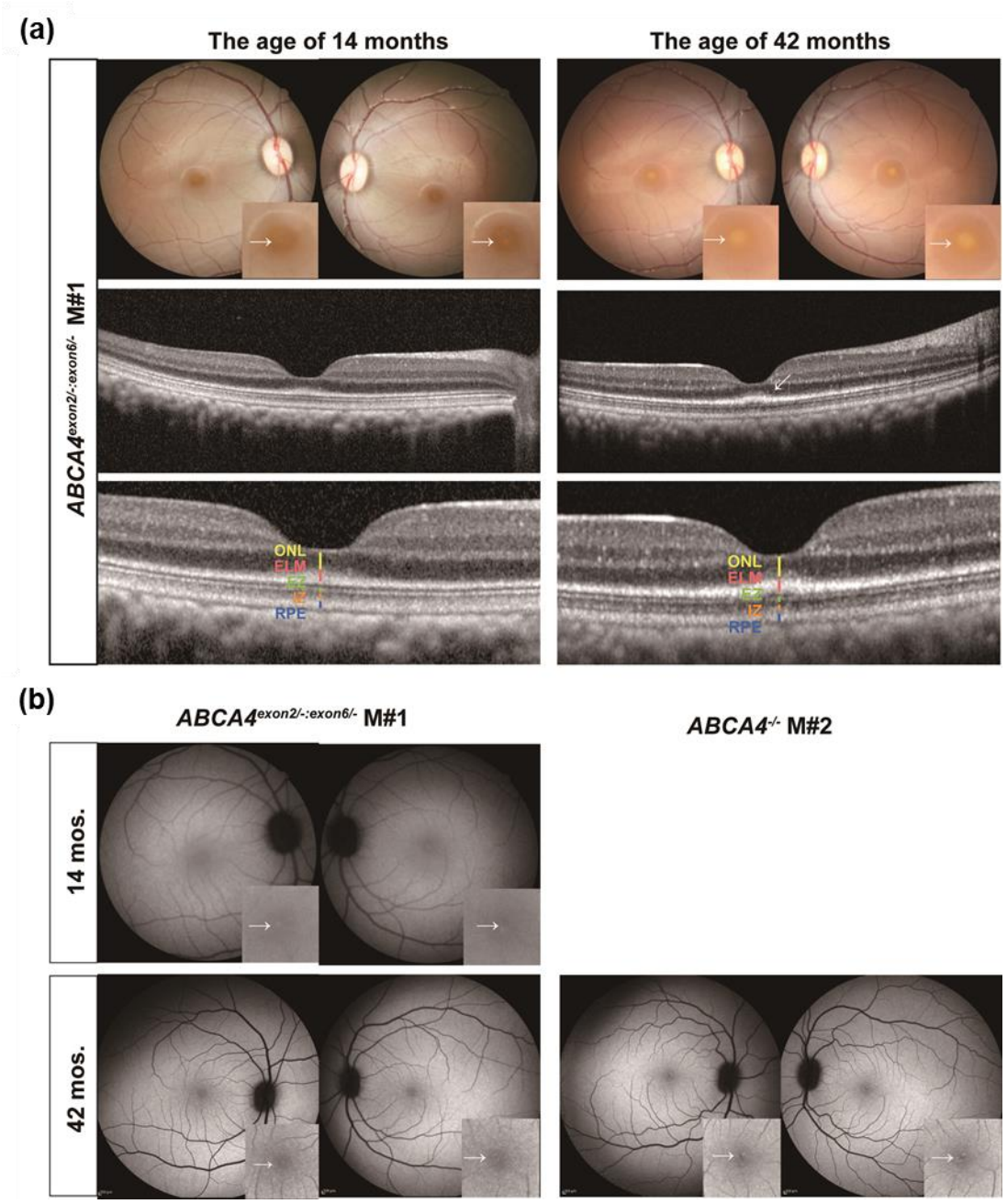

Fig. S5 Fundus photos and OCT imaging of *ABCA4*$^{exon2/-:exon6/-}$ monkey #1 and AF images of *ABCA4* knockout monkeys. (a) Representative fundus photos and OCT images of *ABCA4*$^{exon2/-:exon6/-}$ monkey #1 at the age of 14 months and 42 months. The oval depigmented area and foveal lesion were indicated by arrows. Multiple hyperreflective retinal spots were indicated by arrow on OCT images. Layers on OCT images were indicated in different colors. **(b)** AF images of *ABCA4* knockout

monkeys at the age of 14 months and 42 months. The AF images of *ABCA4*$^{-/-}$ monkey #2 at the age of 14 months was absent due to healthy concern while testing. The vague high autofluorescent fleck and hyperautofluorescent dots at fovea were indicated by arrows.

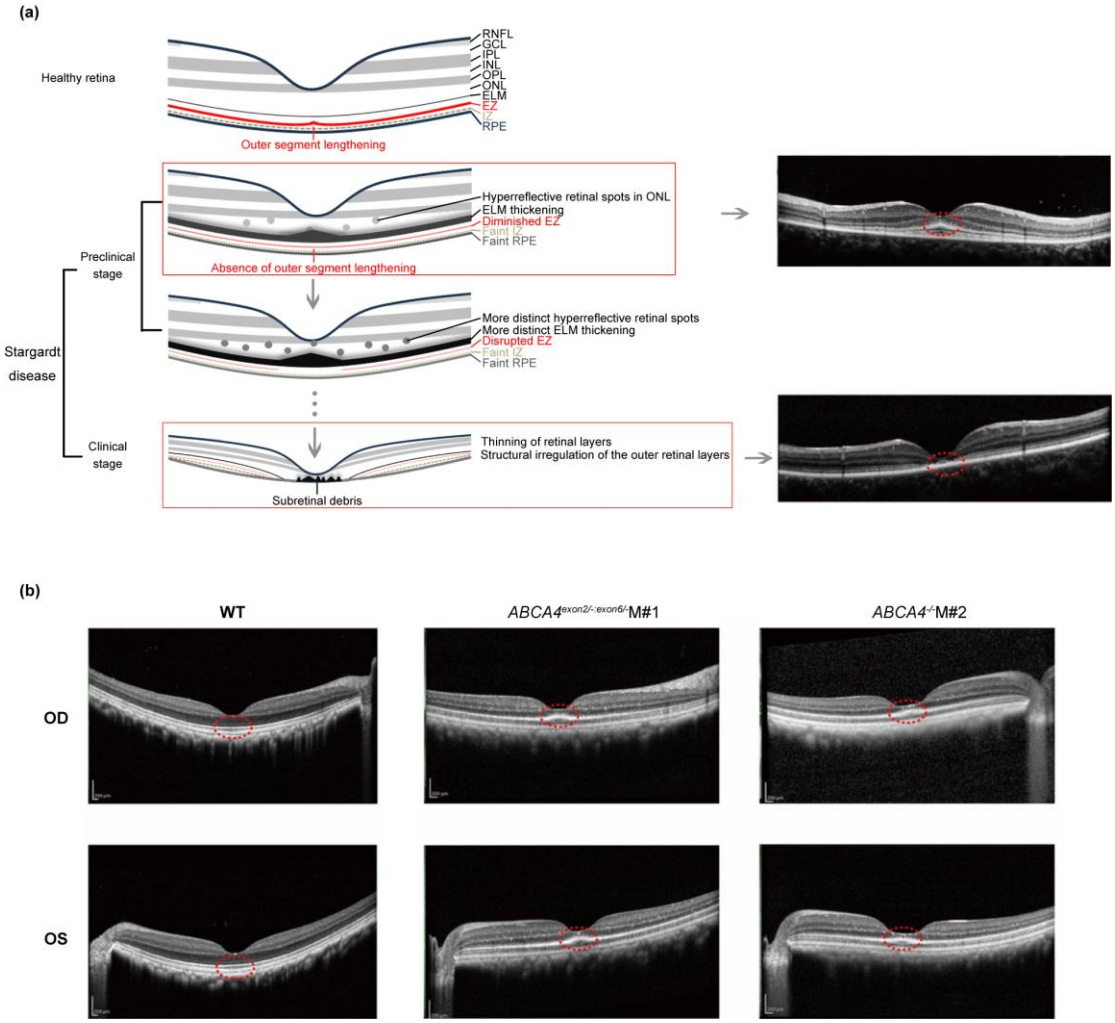

Fig. S6 Clinical manifestation of *ABCA4* defected associated macular degeneration. (a) Diagram for the possible progress pattern of macular degeneration with representative OCT images of *ABCA4*-associated retinopathy patients at different clinical stage. According to the early-stage manifestations of the *ABCA4* knockout monkeys, the ELM thickening, diminished EZ, faint IZ and RPE were first to be observed. Retinal layer structure was preserved at the beginning. Gradually, the retinal

abnormality aggravated, and disruption of outer retina emerged. And then, when the disease progress into clinical stage, obvious disruption of outer retinal layers can be seen. The structure change was highlight in red dotted circle. **(b)** Representative OCT images *ABCA4* KO monkeys and WT monkeys at the age of 14 months(equivalent to 4-5 years old in humans). The fovea was indicated by red dotted circle.

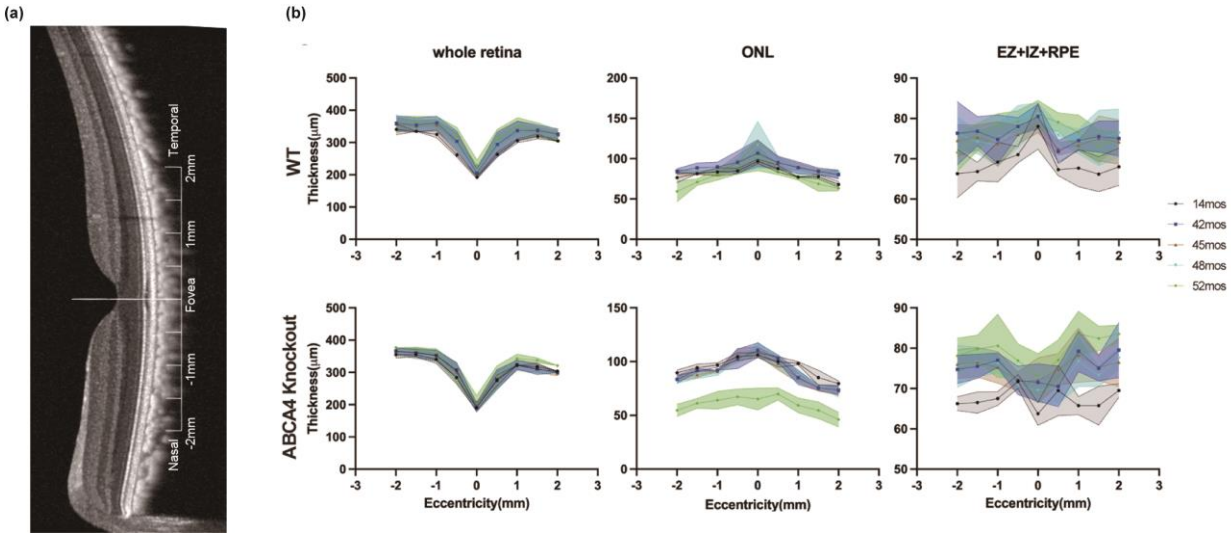

Fig. S7 Measurement of retinal thickness at different age. (a) The diagram for the measurements of retinal layer thickness**.** Retinal layers were measured at the fovea, 0.5mm, 1mm, 1.5mm and 2mm nasal and temporal to fovea. **(b)** Comparison of retinal layer thickness of WT (upper) and *ABCA4* KO (lower) monkeys at different time point. Left**:** Thickness of the whole retina. Middle: Thickness of ONL. Right: Thickness of the layer of EZ+IZ+RPE.

Supplementary tables

Table S1 sgRNA guide sequence

	sgRNA	Guide sequence	PAM
Exon 2	sgRNA1	ATGTTGGCTATAGAGCGGGT	TGG
	sgRNA2	GTTCCACCACAAAGCGAATC	TGG
Exon 6	sgRNA3	CATCTTTAGCCAGCGACGCG	GGG
	sgRNA4	GAGCTTGAAGAAGTCCACGT	TGG

Table S2 CRISPR/Cas9 system injection parameter

Component		Concentration	Final concentration
Cas9-mRNA		766.6ng/μl	100-140ng/μl
sgRNA	sgRNA1	319.8ng/μl	50-60ng/μl
	sgRNA2	280ng/μl	50-60ng/μl
	sgRNA3	326.7ng/μl	50-60ng/μl
	sgRNA4	280ng/μl	50-60ng/μl

Table S3 Embryos test summary

Embryo	Mutation type	efficiency
Embryo-1	Knockout	15/15
Embryo-2	Knockout	15/15
Embryo-3	Knockout	9/9
Embryo-4	Knockout	14/14
Embryo-5	Knockout	15/15
Embryo-6	Pointmutation	14/14
Embryo-7	Knockout	14/14
Embryo-8	Knockout	11/11
Embryo-9	Knockout	8/8
Embryo-10	Knockout	6/6
Embryo-11	Knockout	15/15
Embryo-12	Knockout	15/15
Embryo-13	Knockout	10/10
Embryo-14	Knockout	15/15
Embryo-15	Knockout	15/15
Embryo-16	Knockout and insertion	14/14

Table S4 monkey information

	ID	Date of birth	Gender
KO	192041	2019-12-30	Male
	192042	2019-12-30	Female
WT	190624	2019-09-04	Female
	190607	2019-07-03	Male
	190001	2019-07-24	Male

Table S5 Potential off-target sites in coding region

	Genomic Location	sequence	Overlapping Gene
sgRNA1	16:2982336-2982352	ATGTTGGCTATAGAGC	RAP1GAP2
	13:17573523-17573543	TGTTGGCTATAGAGC	ENSMFAT00000023311
sgRNA2	13:82522663-82522683	CCACCACAAAGCGAATC	BABAM2
	20:56927203-56927223	ACCACAAAGCGAATC	CDH3
	7:165349760-165349780	GTTCCACCACAAAGC	DEGS2
sgRNA4	15:95826085-95826105	GAGCTTGAAGAAGTCCA	NTRK2
	X:14557640-14557660	GAGCTTGAAGAAGTCC	TXLNG
	1:19229227-19229247	GAGCTGGAAGAAGTCCACG	PGBD5
	1:70921466-70921486	CTTGAAGAAGTCCAC	PPP2R5A
	4:56945546-56915566	GCTTGAAGAAGTCCA	PLEKHG1
	3:191715437-191715457	TGAAGAAGTCCACGT	ESYT2
	18:10660494-10660514	TGAAGAAGTCCACGT	DOK6
	18:11261022-11261042	GAGCTTGAAGAAGTC	CCDC102B
	14:96740163-96740183	GAGCTTGAAGAAGTC	ARHGAP42
	8:142336581-142336601	CTTGAAGAAGTCCAC	PTK2
	2:97804711-97804731	CTTGAAGAAGTCCAC	CYP8B1

Table S6 PCR primers

		Sequence	Product length (bP)
Exon2	Nest primer pair 1F	ATATAATAAAACAAGGCAGAGGTTG	425
	Nest primer pair 1R	TACATCGGTCATATGCATCATAGAC	
	Nest primer pair 2F	AAAAGAAGGAAACTGTTTAGGTAAA	314
	Nest primer pair 2R	AAGACCTTTCTAGACAAAAGGC	
Exon6	Nest primer pair 1F	ATTACACAGGGGCCACCTAGA	465
	Nest primer pair 1R	AAGGTCAATTCGTCAGGCTCT	
	Nest primer pair 2F	ATTTTAAAATCAGTTAATTAGTGGC	331
	Nest primer pair 2R	AGTCCACGTTGGCATACAGA	